This is the accepted manuscript made available via CHORUS. The article has been published as:

Topologically Protected Vortex Knots in an Experimentally Realizable System

Hermanni Rajamäki, Toni Annala, and Mikko Möttönen

Phys. Rev. Lett. **133**, 236604 — Published 4 December 2024

DOI: 10.1103/PhysRevLett.133.236604

Topologically Protected Vortex Knots in an Experimentally Realizable System

Hermanni Rajamäki,[1] Toni Annala,[1, 2, 3, *] and Mikko Möttönen[1]

[1] *QCD Labs, QTF Centre of Excellence, Department of Applied Physics, Aalto University, P.O. Box 13500, FI-00076 Aalto, Finland*

[2] *School of Mathematics, Institute for Advanced Study, 1 Einstein Drive, Princeton, 08540, NJ, USA*

[3] *Department of Mathematics, University of Chicago, Eckhart Hall, 5734 S University Ave, Chicago, 60637, IL, USA*

(Dated: November 4, 2024)

Ordered media often support vortex structures with intriguing topological properties. Here, we investigate non-Abelian vortices in tetrahedral order using the mathematical formalism of colored links. Due to the generality of our methods, the results apply to all physical systems governed by tetrahedral order, such as the cyclic phase of spin-2 Bose–Einstein condensates and the tetrahedratic phase of bent-core nematic liquid crystals. Using these vortices, we construct topologically protected knots in the sense that they cannot decay into unlinked simple loop defects through vortex crossings and reconnections without destroying the phase. The discovered structures are the first examples of knots bearing such topological protection in a known experimentally realizable system.

Topological phenomena in physics have attracted persistent attention since Lord Kelvin's vortex-atom theory in 1869 [1], which hypothesized atoms to be knotted vortices in the ether that permeates throughout the cosmos. Since then, interesting topological structures have been discovered in various other contexts: the topologically non-trivial gauge field theory of the Dirac monopole [2], topological defects [3, 4] that appear in various ordered systems such as superfluids [5], Bose–Einstein condensates (BEC) [6, 7], liquid crystals [8–11], and the vacuum structures of quantum field theories [12–14], as well as topological phases of matter such as topological superconductors [15] and topological insulators [16]. Interestingly, such phenomena are amenable to investigation by numerical [17, 18], and experimental means [19–23], resulting in a discipline in which practical experiments and numerical simulations meet methods of abstract topology.

Lord Kelvin's hypothesis on atoms was inspired by the mathematical observation that, in a frictionless ideal fluid, vortex cores cannot pass through each other [1], resulting in a conservation of the knotting type. Thus, knots tied from vortices in such a system behave equivalently to physical knots. In contrast, in ordinary fluids and superfluids, the knot structure of a vortex configuration tends to decay because of strand crossings and local reconnections [24–26].

However, *topological vortices* in ordered media exhibit intermediate stability properties since there exist topological obstructions for strand crossings [27] and local reconnections [28], prompting the question of the stability of knotted structures they form. A topological vortex configuration that cannot decay into a disjoint union of simple, unlinked loops via unobstructed strand crossings and reconnections is referred as being *topologically protected* [28]. This notion highlights the resilience of certain vortex structures, the complexity of which cannot be eliminated by the core-topology-altering evolution that is permitted by the vortex-supporting medium.

Importantly, topological protection is possible only in systems where the order parameter space has a non-Abelian fundamental group; vortices supported by such a medium are known as *non-Abelian vortices*. They occur in numerous physical systems, such as the various phases of spinor Bose–Einstein condensates [6], which have attracted persistent attention owing to their rich topological properties, as well as controllability in laboratory setting [19–23].

Earlier, the topological protection of those topological vortex configurations in the biaxial-nematic [29, 30] and cyclic [31] phases of spin-2 BECs that have no scalar-phase winding about the core was investigated in Ref. [28]. Unfortunately, such vortices do not support any topologically protected knots since a link of at least three components is necessary to achieve topological protection. This requirement of three components is related to the structure of the *quaternion group*

$$Q_8 := \{\pm 1, \pm i, \pm j, \pm k\}, \tag{1}$$

which controls the behavior of the particular class of vortex structures; there is no general mathematical obstruction for the existence of topological vortex knots. In fact, topological vortices controlled by the *permutation group* Σ_3 on three elements exhibit two types of topological vortex knots: the left- and the right-handed tricolored trefoil knot [32]. Unfortunately, no experimentally achievable physical systems which support such vortices has been found.

In this paper, we discover the first topologically protected knot structure in an experimentally realizable order parameter field, namely in the cyclic phase of spin-2 BEC [31]. The behavior of topological vortices in this phase is essentially controlled by the *binary tetrahedral group* [33]

$$T^* := \left\{ \pm 1, \pm i, \pm j, \pm k, \tfrac{\pm 1 \pm i \pm j \pm k}{2} \right\}, \tag{2}$$

which contains 24 elements and the quaternion group Q_8 as a subgroup. In physical terms, the subgroup Q_8 corresponds to the subclass of topological vortices in the cyclic phase of the spin-2 BEC, whereas the group T^* describes the behavior of also those vortices with fractional scalar-phase winding [30, 31]. Interestingly, the binary tetrahedral group also describes topological vortices in the tetrahedratic phase of bent-core nematic liquid crystals [34].

The discovery of topologically protected vortex knots provides fundamental examples highlighting the intricate behaviour of topological structures in realistic physical systems. The link structures discovered previously [28] consist of several vortices, each of which has a distinct vortex type. The topological protection of these structures was predicated [28] on topological obstructions against different vortex types passing through each other. Importantly, the vortex knots we consider consist of a single vortex. Thus its peculiar topological protection is caused by the nontrivial self-interaction of the non-Abelian vortex, a scenario strikingly and fundamentally distinct from previous observations.

Next, we recall the formalism of topological vortices. Let M denote the order parameter space of an ordered medium and $X \subset \mathbb{R}^3$ describe the physical extent of the system. A *topological vortex configuration* consists of a *core* $\mathcal{L} \subset X$, and a continuous map

$$\Psi : X \backslash \mathcal{L} \to M \tag{3}$$

referred to as the *order parameter field*. The core of the defect $\mathcal{L} \subset X$ is assumed to consist of smoothly embedded circles. In other words, $\mathcal{L}$ is a *tame link* [35]. More general one-dimensional core structures, such as embedded graphs, are not considered here for simplicity.

As in Ref. [28], we consider the evolution of the vortex configuration with three types of processes: (i) topology-preserving evolution where the defect-core evolves up to smooth isotopy, and the order parameter field evolves up to homotopy, (ii) *topologically allowed strand crossing* [27] where two cores may cross if they correspond to commuting elements in the *fundamental group* $\pi_1(M)$ of the order parameter space, and (iii) *topologically allowed reconnection* [28] where two vortex cores may reconnect locally if there is no topological obstruction for it. Collectively, the two topology-altering processes are referred to as *topologically allowed modifications*. A topological vortex structure that cannot evolve into a collection of unlinked simple loops via the processes explained above is referred to as being *topologically protected*. Different, but related form of stability of link structures in solitons, based on the Hopf invariant, has been previously investigated [17, 21, 36, 37].

However, the following three types of processes are not considered in our definition of topological protection: (i) non-commuting elements crossing, and forming a rung vortex between the crossing points [27], (ii) loops vanishing by shrinking into a point, and (iii) simple vortices splitting along a significant distance. By simple vortices, we mean singly charged vortices in the sense that the topological charge cannot be expressed as a product of simpler elements of the fundamental group. For example, if the fundamental group is $\mathbb{Z}$, then vortices corresponding to ± 1 are simple, and for the groups Q_8 and T^*, we regard elements that are different from ± 1 as being simple. We physically justify the omission of such events by focusing on low-energy states in low-temperature systems, where such processes are energetically unfavorable. To this end, we also note the following: (i) the energy required to form a rung vortex is linearly proportional to its length in general rendering the formation of long vortex cords unlikely, (ii) in certain BEC systems, ring vortices are protected by an energy barrier against shrinking into a point defect [18], and (iii) the splitting of vortices is energetically unfavourable in some biaxial-nematic liquid crystal systems, and is not observed in simulations [38].

Henceforward, we assume that our physical system is a finite-sized spherical sample of an ordered medium (or at least topologically equivalent to a spherical sample, for example an ellipsoidal sample), and that none of the topological vortices pierce the boundary of the sample. In mathematical terms, the physical extent of the system $X \subset \mathbb{R}^3$ is modelled by the closed unit ball

$$\bar{\mathbb{B}}^3 := \{\mathbf{x} \in \mathbb{R}^3 : ||\mathbf{x}|| \leq 1\} \subset \mathbb{R}^3, \tag{4}$$

and the core link $\mathcal{L}$ is contained in the interior of $\bar{\mathbb{B}}^3$. Under the assumption that the *second homotopy group* $\pi_2(M)$ of the order parameter space M is trivial, a topological vortex configuration may be faithfully represented by a $\pi_1(M)$*-colored link* (Fig. 1), which is a combinatorial object that captures both the topology of the core configuration $\mathcal{L}$, and the homotopy class of the order parameter field $\Psi : X \backslash \mathcal{L} \to M$ [28]. A G-coloring of a link diagram, where G is a group, is an assignment of an element of G (the *color*) to each arc of the diagram such that, at all crossings of the diagram, the color of the undercrossing arc is conjugated by the color of the overcrossing arc as illustrated in Fig. 1. For example, if an arc with color i passes under an arc with color j, its color changes to $jij^{-1} = -i$. The order parameter field Ψ determines a $\pi_1(M)$*-coloring* by assigning to each arc the homotopy class of the path in the order parameter space M traced by Ψ along a path in $X \backslash \mathcal{L}$ that begins from a fixed basepoint above the plane of the picture, travels directly to the base of the arrow, traverses below the arc in the direction of the arrow, and returns back to the basepoint.

The order parameter space for the cyclic phase of spin-2 BEC is

$$M_{\mathrm{C}} = [U(1) \times \mathrm{SO}(3)]/T, \tag{5}$$

where T is the group of the rotational symmetries of a tetrahedron [30, 31]. Furthermore, the fundamental group of $M_{\rm C}$ may be realized as a subgroup of $\mathbb{Z} \times T^*$ where the first component records the fractional scalar-phase winding in multiples of $2\pi/3$. Moreover, for every element of T^* there exists such a choice for the first parameter that the pair is contained in $\pi_1(M_{\rm C})$, and the choice is unique modulo 3. Thus, any T^*-colored link may be constructed as a topological vortex configuration in spin-2 cyclic BEC. Importantly, the theory of colored links [28] may be employed to investigate the existence of topologically protected vortex structures in spin-2 cyclic BEC.

Next, we investigate the topological properties of T^*-colored links. The T^*-colored link diagrams may be graphically presented in terms of bicolored links, as explained in Fig. 2. There are essentially three classes of bicolorings: those corresponding to the elements $\{\pm i, \pm j, \pm k\}$ which we refer to as Q_8 *strands*, those corresponding to elements of the form $(1 \pm i \pm j \pm k)/2$ which we refer to as *black strands*, and those corresponding to elements of the form $(-1 \pm i \pm j \pm k)/2$ which we refer to as *gray strands*. The crossing rules in T^*-colored link diagrams shown in Fig. 3 can be understood in terms of rotations of a decorated tetrahedron (see the Supplemental Material). Topologically allowed modifications admit a graphical presentation as well, as explained in Fig. 4.

In order to verify the topological protection of a vortex configuration, we construct invariants of T^*-colored links that are conserved in topologically allowed modifications, and for which a configuration of unlinked simple loops obtains a trivial value. Hence, a non-zero value of the invariant is a sufficient, but not necessary condition for topological protection.

We introduce two invariants, Q_b and Q_g, which are computed using the black strands, and the gray strands, respectively. These invariants are similar to the Q-invariant defined in Ref. [28].

The invariant $Q_g \in \mathbb{Z}_6$ for gray loops is defined by first interchanging the corresponding black and gray bicolorings, and then computing the invariant $Q_b \in \mathbb{Z}_6$ for black loops, the definition of which we explain next. Each black and gray loop has an orientation, i.e., a preferred direction, such that the black or the gray color of the bicoloring is on the right side when traversing along the loop according to the orientation. For each black loop L of the diagram, we choose a basepoint b on one of the arcs of L in the diagram, and define $q(L, b) \in T^*$ as the product of elements one obtains when L crosses under other strands and itself, in the order the crossings occur along L, from right to left. The element $q(L, b)$ is a power of the element $\chi(b)$ corresponding to the coloring at the basepoint,

$$q(L, b) = \chi(b)^{Q'(L)}, \tag{6}$$

and the exponent $Q'(L) \in \mathbb{Z}_6$ is independent of the choice of the basepoint, and is well-defined modulo 6 (see Appendix A). The black invariant is then defined as

$$Q_b := \sum_{L \text{ is a black loop}} Q'(L) - \omega_b - 4l_{bg} \in \mathbb{Z}_6, \tag{7}$$

where ω_b is the signed count of undercrossings where both strands are black, and l_{bg} is the signed count of crossings where a black strand crosses under a gray strand (Fig. 5). The sign of each crossing is decided by the right-hand rule (see Appendix A).

The invariants Q_b and Q_g are conserved in topologically allowed local modifications (see Appendix A). Thus, under our earlier assumption that the vortex core structure only evolves by topologically allowed local modifications, Q_b and Q_g are conserved in the dynamics of the system. Clearly, these invariants vanish for a configuration of unlinked simple loops. A non-zero value of either invariant therefore implies a topologically protected structure: the link cannot decay into unlinked simple loops by the processes described above. However, we suspect that the invariants are not complete in the sense that structures with identical invariants may not necessarily be topologically equivalent as exemplified in Fig. 6.

The topological invariants defined above demonstrate that topologically protected knots and links exist in the cyclic phase of spin-2 BEC. Two T^*-colored knot structures, the trefoil and the figure-eight knot, illustrated in Fig. 6(a), have invariant $Q_b = [3]$. The winding of the tetrahedral field at various points of the topologically protected trefoil is depicted in Fig. 7. Equivalent knots can be constructed using gray loops, with $Q_g = [3]$. Fig. 6(b) demonstrates the existence of a topologically protected link consisting of one black and one gray loop. The T^*-colored trefoil and figure-eight knots differ by a black Solomon's link structure which is a T^*-colored link consisting of two black loops. In the Supplemental Material, we show that every T^*-colored link structure consisting of only black loops decomposes into unlinked configurations of T^*-colored trefoil and figure-eight knots. Hence, the knots displayed in Fig. 6(a) can be regarded as building blocks of purely black T^*-colored link structures consisting of only black strands. By symmetry, an equivalent statement is true for purely gray T^*-colored link structures. No such decomposition theorems are known for structures containing different types of loops.

In conclusion, we studied topologically intriguing vortex structures in the cyclic phase of spin-2 BEC and in bent-core nematic liquid crystals, by employing the mathematical theory of T^*-colored links, which allows representing tetrahedral order parameter fields with simple diagrams. We have also explicitly written down and visualized the order parameter field of a topologically protected trefoil knot in Spin-2 BEC in Appendix B. Due to the generality of our formalism, it may also be applicable in a wide range of other physical systems in condensed-matter and high-energy physics. We provide

the first examples of topologically protected vortex knots that are in principle experimentally realizable.

Our results leave several interesting questions open, such as the detailed method to realize the proposed vortex structures in practice using experimentally available control techniques. This is a challenging task since topologically protected knots cannot, by definition, be manufactured by performing local surgeries to an unknotted loop defect, which is a method that has been applied successfully in the case of colloidal particles [39]. A rapid phase transition may generate a random vortex structure [40]; however, it often results in a vortex network characterized by multiple junction points where three vortex lines meet, rather than a vortex link [38]. Alternatively, controlled tailoring of electromagnetic or other fields that would induce the desired structure in the condensate, in the spirit of of [20, 41, 42], could be pursued. On the theoretical side, the complete classification T^*-colored links up to topological modifications remains open.

We thank T. Machon for pointing out that the tetrahedral order arises in bent-core nematic liquid crystals. We have received funding from the Academy of Finland Centre of Excellence program (Project No. 336810) and from the National Science Foundation (Grant No. DMS-1926686). T.A. thanks IAS for excellent working conditions.

APPENDIX A: Q-INVARIANTS

Here, we prove that the invariants Q_b and Q_g, collectively referred to as the *Q-invariants*, used in the main text are well defined and conserved in topologically allowed local surgeries. Thus, they can be employed to detect topological protection. A more comprehensive treatment of the Q-invariants, including comparison with the invariant defined in Ref. [28], is provided in the Supplemental Material.

In a T^*-colored link diagram, every black and gray loop has a canonical *orientation*, i.e., a preferred direction, which is defined to be the direction for which the black or gray color of the bicoloring is on the right side. If b is a point on one of the arcs of a loop L, then $\chi(b) \in T^*$ is the color of L at b, and $q(L,b) \in T^*$ is the product of the colors of the arcs one passes under when traversing along L in the direction of the orientation starting from b (Fig. 5). Importantly, in the product defining $q(L,b)$, the colors are multiplied in reverse order to the sequence in which they are encountered during the traversal.

Lemma 1. *If L is a black loop, then the element $q(L,b)$ is a power of $\chi(b)$.*

Proof. For the coloring of the loop L to be consistent, $q(L,b)$ must commute with $\chi(b)$. Since the only elements of T^* that commute with an element of form $(1 \pm i \pm j \pm k)/2$ are powers of that element, the claim follows. □

Thus, for black loops L,

$$q(L,b) = \chi(b)^{Q'(L,b)} \tag{8}$$

and the exponent $Q'(L,b)$ is an integer that is well defined modulo 6.

Lemma 2. *$Q'(L,b) \in \mathbb{Z}_6$ is independent of the basepoint b.*

Proof. It suffices to show that $Q'(L,b) = Q'(L,b')$, where b' is a basepoint on the arc one reaches after single undercrossing when traversing L from b according to the orientation. Let $a \in T^*$ be the color of the undercrossing. Then

$$\chi(b') = a\chi(b)a^{-1} \tag{9}$$

$$q(L,b') = aq(L,b)a^{-1}. \tag{10}$$

As conjugation by a is a group homomorphism,

$$\chi(b')^{Q'(L,b')} = \chi(b')^{Q'(L,b)}. \tag{11}$$

Thus $Q'(L,b') \equiv Q'(L,b) \mod 6$, as desired. □

Henceforth, we will use simpler notation $Q'(L)$. The black invariant is defined by the formula

$$Q_b := \sum_{L \text{ is a black loop}} Q'(L) - \omega_b - 4l_{bg} \in \mathbb{Z}_6, \tag{12}$$

where ω_b is the signed count of undercrossings where both strands are black, and l_{bg} is the signed count of crossings where a black strand crosses under a gray strand. The sign of a crossing is determined by the right hand rule (Fig. 8).

Next, we prove that the Q-invariants remain invariant under Reidemeister moves (Fig. 9). In other words, the Q-invariants depend only on the T^*-colored link rather than the specific diagram representing it.

Lemma 3. *The Q-invariants are conserved under Reidemeister moves.*

Proof. Reidemeister moves of type II and III clearly do not affect any of the $Q'(L)$. Moreover, if a move of type I is applied on a loop L, the effects to $Q'(L)$ and ω_b cancel each other. Thus, in all cases the Q-invariants remain unchanged. □

Finally, the following two lemmas show that the Q-invariants are conserved in topologically allowed local surgeries.

Lemma 4. *The Q-invariants are conserved in topologically allowed local strand crossings.*

Proof. There are three kinds of strand crossings to consider: (i) the two strands are part of the same loop, (ii) the strands are part of different loops, both of which are black, and (iii) one of the strands is black and the other is gray. In each case, the effects on the $Q'(L)$, ω_b, and l_{bg} cancel each other, leaving the Q-invariants unchanged. Case (i) is illustrated in detail in Fig. 10. □

Lemma 5. *The Q-invariants are conserved in topologically allowed local reconnections.*

Proof. If two strands that are part of the same black loop reconnect, the loop splits into two loops because the reconnection is compatible with the orientation of the loop. Conversely, if two black strands that are part of different loops reconnect, they combine into a single loop. By symmetry, it suffices to consider the effect on Q_b of two loops L and L' amalgamating into L''.

Since $Q(L'') = Q(L) + Q(L')$ and the other ingredients in the definition of Q_b remain unchanged, Q_b remains unchanged in the reconnection. □

We conclude by stating explicitly the implication of the above results.

Theorem 6 (Q-invariants detect topological protection)**.** *If $\mathcal{L}$ is a T^*-colored link such that at least one of the invariants Q_b or Q_g is non-zero, then $\mathcal{L}$ is topologically protected.*

Proof. The invariants of a collection of simple, unlinked loops are 0. Thus, by Lemmas 4 and 5, non-zero invariant implies that the colored link $\mathcal{L}$ cannot be decomposed into such a collection using topologically allowed local surgeries. In other words, $\mathcal{L}$ is topologically protected. □

APPENDIX B: ORDER PARAMETER FIELD OF A TOPOLOGICALLY PROTECTED TREFOIL KNOT IN SPIN-2 BEC

Here, we write the order parameter field surrounding a topologically protected trefoil knot in the cyclic phase of a spin-2 BEC. Following Refs. [31, 43], an $F = 2$ spinor is a symmetric and traceless 3×3 complex matrix.

The matrix

$$\Psi_0 = \frac{1}{\sqrt{6}} \begin{bmatrix} 1 & 0 & 0 \\ 0 & \omega & 0 \\ 0 & 0 & \omega^2 \end{bmatrix} \tag{13}$$

is a ground state for the cyclic phase of spin-2 BEC [31], where $\omega = e^{2\pi i/3}$. The full ground-state manifold is obtained by applying symmetry transformations: three dimensional rotations and $U(1)$-gauge transformations. In general, the full ground-state manifold is parametrized by

$$\Psi = \lambda \cdot O\Psi_0 O^T, \tag{14}$$

where λ is a unit complex number, and $O \in \mathrm{SO}(3)$ [30, 31].

The ground-state manifold for the cyclic phase is the quotient space

$$M_C = [U(1) \times \mathrm{SO}(3)]/T, \tag{15}$$

where the stabilizer of Ψ_0 is the tetrahedral group T that is generated by the diagonal matrices $I_x = \mathrm{diag}(1, -1, -1)$, $I_y = \mathrm{diag}(-1, 1, -1)$, and $I_z = \mathrm{diag}(-1, -1, 1)$, together with the cyclic matrix

$$\mathcal{C} = \begin{bmatrix} 0 & 1 & 0 \\ 0 & 0 & 1 \\ 1 & 0 & 0 \end{bmatrix} \tag{16}$$

accompanied by a phase $\lambda = e^{-2\pi i/3}$.

From Eq. 15, one obtains a description of the fundamental group of M_C as a subgroup, $\pi_1(M_C, \Psi_0) \subset \mathbb{Z} \times T^*$, where T^* accounts for the winding of the spin-degree of freedom, and $\mathbb{Z}$ for the winding of global phase in multiples of $2\pi/3$. A loop in M_C corresponding to the element $(1 - i - j - k)/2$ can be obtained by acting on Ψ_0 with

$$\left(e^{-\frac{4i}{3}t}, \begin{bmatrix} \cos^2 t & \sin t & -\frac{1}{2}\sin 2t \\ -\frac{1}{2}\sin 2t & \cos t & \sin^2 t \\ \sin t & 0 & \cos t \end{bmatrix} \right) \tag{17}$$

as t ranges from 0 to $\pi/2$. Similarly, loops corresponding to $(1-i+j+k)/2$, $(1+i-j+k)/2$, and $(1+i+j-k)/2$, can be obtained by conjugating the second argument by I_x, I_y, and I_z, respectively.

Next, we write down an example of an order parameter field on a torus surrounding a topologically protected trefoil knot in spin-2 BEC (see Fig. 7). Denoting by s the longitudinal parameter that ranges from 0 to $3\pi/2$ and ϕ the latitudinal coordinate that ranges from 0 to 2π, we define

$$\Psi_{\mathrm{trefoil}}(s, \phi) = e^{i\phi/3} \cdot O(s, \phi)\Psi_0 O(s, \phi)^T, \tag{18}$$

where $O(s, \phi) = B(s)A(\phi)$,

$$A(\phi) = \begin{bmatrix} \cos^2(-\frac{\phi}{4}) & \sin(-\frac{\phi}{4}) & \frac{1}{2}\sin(-\frac{\phi}{2}) \\ -\frac{1}{2}\sin(-\frac{\phi}{2}) & \cos(-\frac{\phi}{4}) & -\sin^2(-\frac{\phi}{4}) \\ -\sin(-\frac{\phi}{4}) & 0 & \cos(-\frac{\phi}{4}) \end{bmatrix} \tag{19}$$

and finally,

$$B(s) = \begin{cases} \begin{bmatrix} \cos^2 s & -\sin s & -\frac{1}{2}\sin 2s \\ \frac{1}{2}\sin 2s & \cos s & -\sin^2 s \\ \sin s & 0 & \cos s \end{bmatrix} & \text{if } s \in [0, \pi/2]; \\ \begin{bmatrix} \cos^2(s-\frac{\pi}{2}) & \sin(s-\frac{\pi}{2}) & \frac{1}{2}\sin(2s-\pi) \\ -\frac{1}{2}\sin(2s-\pi) & \cos(s-\frac{\pi}{2}) & -\sin^2(s-\frac{\pi}{2}) \\ -\sin(s-\frac{\pi}{2}) & 0 & \cos(s-\frac{\pi}{2}) \end{bmatrix} \begin{bmatrix} 0 & -1 & 0 \\ 0 & 0 & -1 \\ 1 & 0 & 0 \end{bmatrix} & \text{if } s \in [\pi/2, \pi]; \\ \begin{bmatrix} \cos^2(s-\pi) & -\sin(s-\pi) & \frac{1}{2}\sin(2s-2\pi) \\ \frac{1}{2}\sin(2s-2\pi) & \cos(s-\pi) & \sin^2(s-\pi) \\ -\sin(s-\pi) & 0 & \cos(s-\pi) \end{bmatrix} \begin{bmatrix} 0 & 0 & -1 \\ -1 & 0 & 0 \\ 0 & 1 & 0 \end{bmatrix} & \text{if } s \in [\pi, 3\pi/2]. \end{cases} \tag{20}$$

In the coloring scheme of Fig. 2, $A(\phi)$ corresponds to a yellow-black vortex traversed in the inverse direction, and the three pieces of $B(s)$ correspond to green-black, yellow-black, and salmon-black vortices, respectively.

* tannala@ias.edu

[1] W. Thomson, On vortex atoms, Proceedings of the Royal Society of Edinburgh **6**, 94 (1869).

[2] P. Dirac, Quantised singularities in the electromagnetic field,, Proceedings of the Royal Society of London. Series A, Containing Papers of a Mathematical and Physical Character **133**, 60 (1931).

[3] G. E. Volovik and V. P. Mineev, Investigation of singularities in superfluid he^3 in liquid crystals by the homotopic topology methods, Sov. Phys. - JETP (Engl. Transl.); (United States) **45:6** (1977).

[4] N. D. Mermin, The topological theory of defects in ordered media, Reviews of Modern Physics **51**, 591 (1979).

[5] G. E. Volovik, *The Universe in a Helium Droplet* (Oxford University Press, 2009).

[6] Y. Kawaguchi and M. Ueda, Spinor bose–einstein condensates, Physics Reports **520**, 253 (2012).

[7] M. Ueda, Topological aspects in spinor bose–einstein condensates, Reports on Progress in Physics **77**, 122401 (2014).

[8] T. Machon and G. P. Alexander, Knots and nonorientable surfaces in chiral nematics, Proceedings of the National Academy of Sciences **110**, 14174 (2013).

[9] D. A. Beller, T. Machon, S. Čopar, D. M. Sussman, G. P. Alexander, R. D. Kamien, and R. A. Mosna, Geometry of the cholesteric phase, Physical Review X **4**, 031050 (2014).

[10] T. Machon and G. P. Alexander, Umbilic lines in orientational order, Physical Review X **6**, 011033 (2016).

[11] T. Machon, H. Aharoni, Y. Hu, and R. D. Kamien, Aspects of defect topology in smectic liquid crystals, Communications in Mathematical Physics **372**, 525 (2019).

[12] M. Bucher, H.-K. Lo, and J. Preskill, Topological approach to alice electrodynamics, Nuclear Physics B **386**, 3 (1992).

[13] M. Bucher, K.-M. Lee, and J. Preskill, On detecting discrete cheshire charge, Nuclear Physics B **386**, 27 (1992).

[14] M. Bucher and A. S. Goldhaber, SO(10) cosmic strings and $SU(3)_{\text{color}}$ Cheshire charge, Physical Review D **49**, 4167 (1994).

[15] M. Sato and Y. Ando, Topological superconductors: a review, Reports on Progress in Physics **80**, 076501 (2017).

[16] M. Z. Hasan and C. L. Kane, Colloquium: Topological insulators, Reviews of Modern Physics **82**, 3045 (2010).

[17] L. Faddeev and A. J. Niemi, Stable knot-like structures in classical field theory, Nature **387**, 58 (1997).

[18] J. Ruostekoski and J. R. Anglin, Monopole core instability and alice rings in spinor bose-einstein condensates, Physical Review Letters **91**, 190402 (2003).

[19] M. W. Ray, E. Ruokokoski, S. Kandel, M. Möttönen, and D. S. Hall, Observation of dirac monopoles in a synthetic magnetic field, Nature **505**, 657 (2014).

[20] M. W. Ray, E. Ruokokoski, K. Tiurev, M. Mottonen, and D. S. Hall, Observation of isolated monopoles in a quantum field, Science **348**, 544 (2015).

[21] D. S. Hall, M. W. Ray, K. Tiurev, E. Ruokokoski, A. H. Gheorghe, and M. Möttönen, Tying quantum knots, Nature Physics **12**, 478 (2016).

[22] W. Lee, A. H. Gheorghe, K. Tiurev, T. Ollikainen, M. Möttönen, and D. S. Hall, Synthetic electromagnetic knot in a three-dimensional skyrmion, Science Advances **4**, 10.1126/sciadv.aao3820 (2018).

[23] A. Blinova, R. Zamora-Zamora, T. Ollikainen, M. Kivioja, M. Möttönen, and D. S. Hall, Observation of an Alice ring in a Bose–Einstein condensate, Nature Communications **14**, 10.1038/s41467-023-40710-2 (2023).

[24] D. Kleckner and W. T. M. Irvine, Creation and dynamics of knotted vortices, Nature Physics **9**, 253 (2013).

[25] D. Kleckner, M. W. Scheeler, and W. T. M. Irvine, The life of a vortex knot, Physics of Fluids **26**, 091105 (2014).

[26] D. Kleckner, L. H. Kauffman, and W. T. M. Irvine, How superfluid vortex knots untie, Nature Physics **12**, 650 (2016).

[27] V. Poenaru and G. Toulouse, The crossing of defects in ordered media and the topology of 3-manifolds, Journal de Physique **38**, 887 (1977).

[28] T. Annala, R. Zamora-Zamora, and M. Möttönen, Topologically protected vortex knots and links, Communications Physics **5**, 10.1038/s42005-022-01071-2 (2022), arXiv:2204.03612 [cond-mat.quant-gas].

[29] J. L. Song, G. W. Semenoff, and F. Zhou, Uniaxial and biaxial spin nematic phases induced by quantum fluctuations, Physical Review Letters **98**, 160408 (2007).

[30] A. M. Turner, R. Barnett, E. Demler, and A. Vishwanath, Nematic order by disorder in spin-2 Bose–Einstein condensates, Physical Review Letters **98**, 190404 (2007).

[31] G. W. Semenoff and F. Zhou, Discrete symmetries and 1/3-quantum vortices in condensates of F=2 cold atoms, Physical Review Letters **98**, 100401 (2007).

[32] T. Annala, H. Rajamäki, and M. Möttönen, Bordism invariants of colored links and topologically protected tricolorings (2023), arXiv:2301.09532 [math.GT].

[33] M. Golasiński and D. L. Gonçalves, Automorphism groups of generalized (binary) icosahedral, tetrahedral and octahedral groups, Algebra Colloquium **18**, 385 (2011).

[34] T. C. Lubensky and L. Radzihovsky, Theory of bent-core liquid-crystal phases and phase transitions, Physical Review E **66**, 031704 (2002).

[35] D. Rolfsen, *Knots and links* (AMS Chelsea Pub, Providence, R.I, 2003).

[36] E. Babaev, L. D. Faddeev, and A. J. Niemi, Hidden symmetry and knot solitons in a charged two-condensate Bose system, Physical Review B **65**, 100512 (2002).

[37] F. N. Rybakov, J. Garaud, and E. Babaev, Stable Hopf-Skyrme topological excitations in the superconducting state, Physical Review B **100**, 094515 (2019).

[38] N. V. Priezjev and R. A. Pelcovits, Coarsening dynamics of biaxial nematic liquid crystals, Physical Review E **66**, 051705 (2002).

[39] U. Tkalec, M. Ravnik, S. Copar, S. Zumer, and I. Musevic, Reconfigurable knots and links in chiral nematic colloids, Science **333**, 62 (2011).

[40] D. Seč, S. Čopar, and S. Žumer, Topological zoo of free-standing knots in confined chiral nematic fluids, Nature Communications **5**, 10.1038/ncomms4057 (2014).

[41] T. Ollikainen, K. Tiurev, A. Blinova, W. Lee, D. Hall, and M. Möttönen, Experimental Realization of a Dirac Monopole through the Decay of an Isolated Monopole, Physical Review X **7**, 021023 (2017).

[42] V. Pietilä and M. Möttönen, Creation of dirac monopoles in spinor bose-einstein condensates, Physical Review Letters **103**, 030401 (2009).

[43] F. Zhou and G. W. Semenoff, Quantum Insulating States of $F = 2$Cold Atoms in Optical Lattices, Physical Review Letters **97**, 10.1103/physrevlett.97.180411 (2006).

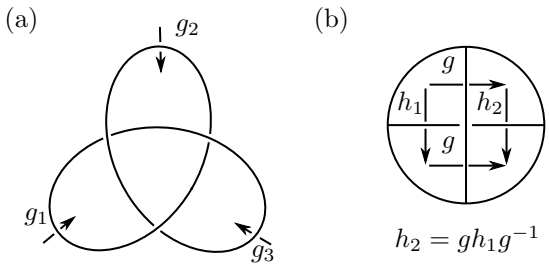

FIG. 1. ***G*-colored link diagrams.** G-coloring of a link diagram is an assignment of an element of a group G (the color) to each arc of the diagram (a), such that at each crossing of the diagram, the color of the undercrossing arc changes by conjugating it with the color of the overcrossing arc (b).

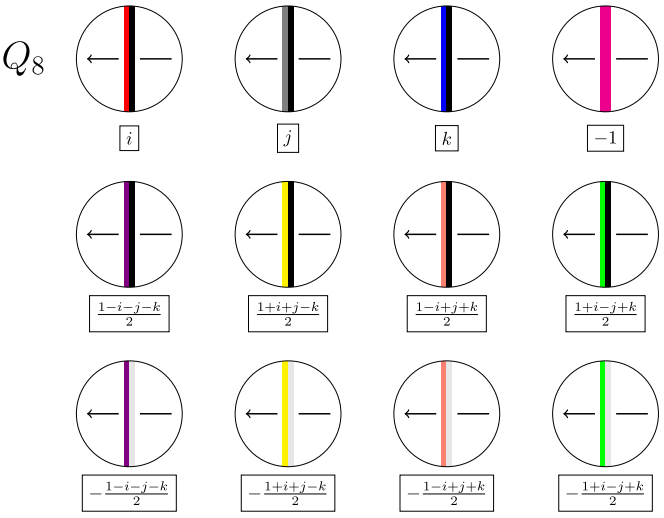

FIG. 2. **$\mathbf{T}^*$-colored link diagrams: coloring scheme.** The cores of the topological vortices are represented by bicolored arcs, except the element $\{-1\}$, which is represented by a singly-colored arc. Crossing under the strand in the opposite direction corresponds to the inverse element in T^*, which coincides with the conjugate quaternion. The elements of the bottom and the middle row form conjugacy classes of four elements each. The elements of the top row, as well as their inverses, form the normal subgroup $Q_8 \subset T^*$. The identity element does not correspond to a topological vortex.

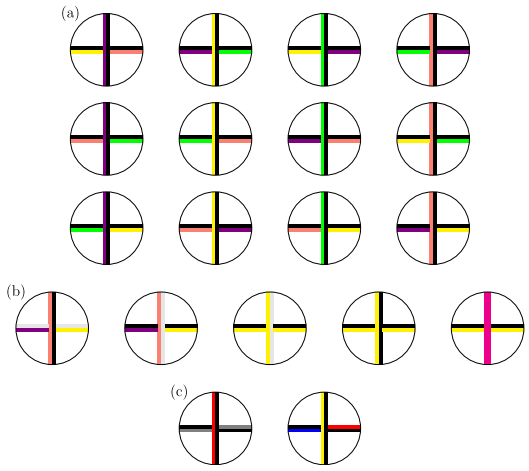

FIG. 3. **$\mathbf{T^*}$-colored link diagrams: crossing rules.** (a) Complete crossing rules between the black strands. The color changes in the undercrossing, but the direction of the bicoloring remains unchanged. (b) Passing under a strand with an identical colored part of the bicoloring, or a purple strand, does not change the bicoloring. A bicoloring with gray colored part behaves identically to the corresponding black bicoloring in crossings, because the group elements differ by the multiplication by the element -1 which commutes with every element of T^*. (c) In a Q_8-colored diagram, the bicoloring is flipped when passing under another bicolored strand in Q_8. When passing under a strand that does not belong to the subgroup Q_8, the bicoloring does not necessarily flip and the color may change.

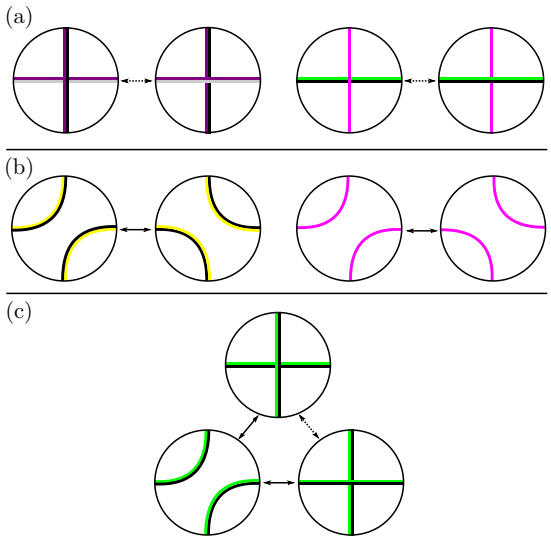

FIG. 4. **Topologically allowed local modifications.** The two types of local modifications considered, strand crossings and reconnections, are marked by dashed and solid arrows respectively. (a) Strand crossings may occur between strands having identical colored parts of the bicoloring, as well as between a purple strand and any other strand. (b) Reconnections may only occur between strands with identical bicolorings. (c) A crossing between the bicolored strands of the same kind may be modified with both the strand crossing and reconnection.

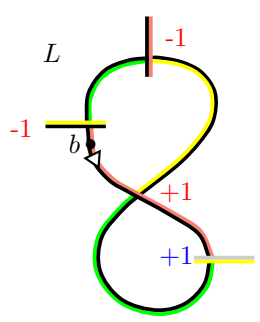

$$q(L,b) = -\tfrac{1}{16}(1-i-j+k) \times (1+i-j-k) \times (1-i+j+k) \times (1+i+j-k) = -1$$

$$\chi(b) = \tfrac{1}{2}(1-i+j+k)$$

$$Q'(L) = 3 \in \mathbb{Z}_6$$

FIG. 5. **Computation of $Q'(L)$ and Q_b.** Example computation of the $Q'(L)$-invariant for a black loop L in a T^*-colored link diagram. The contributions of the displayed crossings to ω_b and l_{bg} are also marked in the figure by red and blue text, respectively.

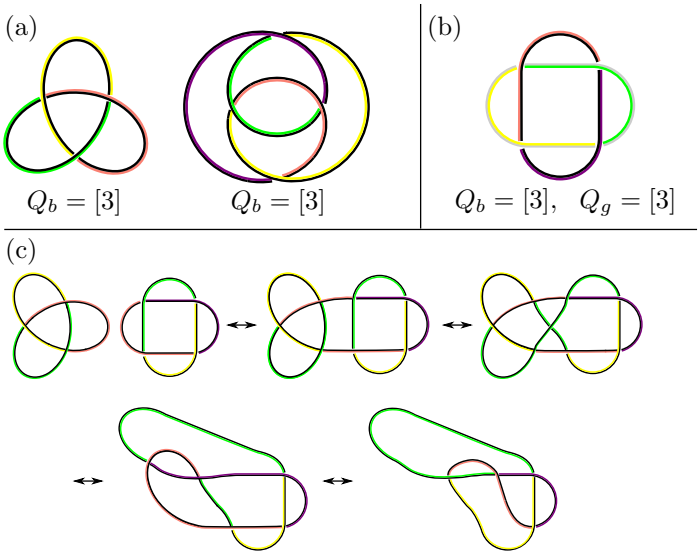

FIG. 6. **Examples of topologically protected T*-colored knots and links.** (a) Topologically protected T^*-colored trefoil knot and figure-eight knot and the values of their invariants. (b) Topologically protected T^*-colored Solomon's link, tied from one black and one gray loop. (c) A trefoil may be turned into a figure-eight knot by combining it with a T^*-colored Solomon's link consisting of two black loops. The black Solomon's link has trivial invariants, but it is unknown if it is topologically protected or not. Hence, even though the T^*-colored trefoil and the figure-eight knot have equivalent invariants, it is unknown if they can be turned into each other by topologically allowed modifications.

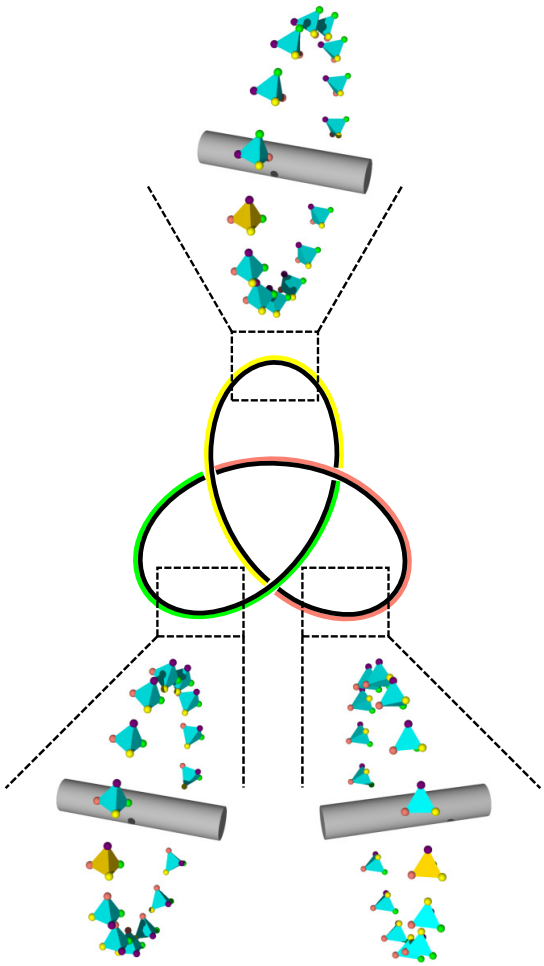

FIG. 7. **Order parameter field of a topologically protected trefoil.** Winding of the tetrahedral field at various points of the topologically protected trefoil knot. Colored dots have been added to the vertices of the tetrahedron to make it easier to distinguish between different rotations. Furthermore, the colors correspond to the element of T^*, in the coloring scheme of Fig. 2, that is obtained when rotating the tetrahedron by 120 degrees about the axis of the vertex according to the right hand rule. Golden tetrahedron signifies the basepoint of the loop.

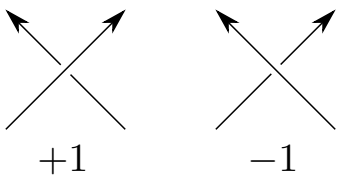

FIG. 8. **Writhe.** Sign of an oriented crossing is determined by the right hand rule.

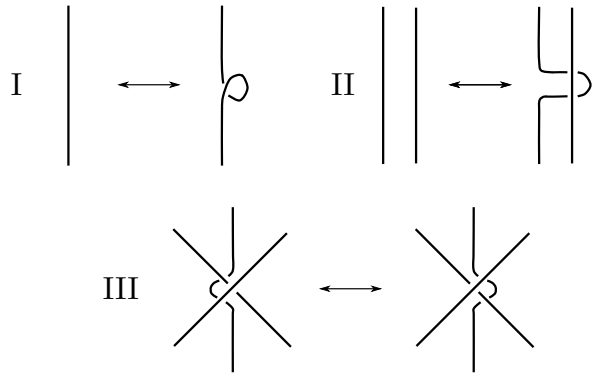

FIG. 9. **Reidemeister moves.** Any two link diagrams representing the same link can be related by a sequence of Reidemeister moves, of which there are three types.

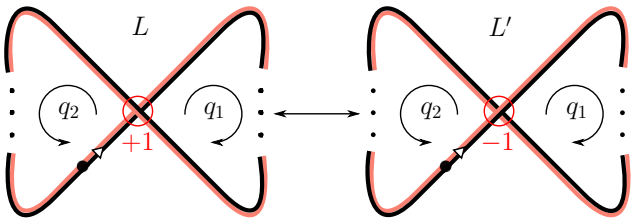

$$Q'(L) + 1 = Q'(L') - 1$$

FIG. 10. **Topologically allowed crossing.** Example of topologically allowed crossing of strands belonging to the same loop L. The effects on $Q'(L)$ and ω_b cancel each other, leaving the Q-invariant unchanged.